Journal of Physics: Conference Series

PAPER • OPEN ACCESS

Multi-fidelity actuator-line modelling of FOWT wakes

To cite this article: Agnese Firpo *et al* 2024 *J. Phys.: Conf. Ser.* **2767** 052050

Multi-fidelity actuator-line modelling of FOWT wakes

Agnese Firpo[1], Andrea G Sanvito[1], Giacomo Persico[1], Vincenzo Dossena[1], Paolo Schito[2], Alberto Zasso[2]

[1] Department of Energy, Politecnico di Milano, Via Lambruschini 4, Milano, 20156, Italy
[2] Department of Mechanical Engineering, Politecnico di Milano, Via La Masa 1, Milano, 20156, Italy

E-mail: agnese.firpo@polimi.it (Agnese Firpo), andreagiuseppe.sanvito@polimi.it (Andrea G. Sanvito), giacomo.persico@polimi.it (Giacomo Persico), vincenzo.dossena@polimi.it (Vincenzo Dossena) paolo.schito@polimi.it (Paolo Schito), alberto.zasso@polimi.it(Alberto Zasso)

Abstract. Large Eddy Simulations (LES) are considered the proper tool for predicting the physics of a wind turbine wake, thereby establishing a solid foundation for investigating the interaction among floating turbines within wind farms. In this work the Actuator Line Model, implemented in the OpenFoam environment, is combined with both U-RANS and LES simulations to underline the differences in accuracy when reproducing the near and far wake of a single turbine. Both a fixed-bottom and a surge motion case are tested to highlight the wake phenomena strictly generated by the platform motion. The use of LES simulation becomes fundamental by virtue of its ability to accurately simulate turbulence and mixing with free-stream flow, hence, this research aims at advancing the knowledge of wake dynamics from multiple perspectives while ensuring reliability thanks to the use of the experimental wake data from the UNAFLOW test campaign on the scaled laboratory model of the DTU 10 MW. In the near wake, limited flow unsteadiness and similar mean velocity are predicted by the two models. In the far wake, instead, the LES approach estimates a strong rise of flow unsteadiness which, in case of surge motion, affects the mean velocity value making evident the difference between LES and RANS estimation.

1. Introduction

To enhance the efficiency of floating offshore wind farms, it is imperative to investigate the turbine wake evolution before studying the interactions among different turbines. Floating offshore wind turbines (FOWTs) are influenced by the combined forces of wind and waves, leading to fluctuating movements that give rise to unsteady aerodynamic phenomena including wake meandering, wake velocity pulsations, tip-vortex unsteadiness; all these phenomena contribute to alter the mixing in the far wake and the wake recovery with respect to fixed-bottom turbine configurations.

To reliably model such wake features, Computational fluid dynamics (CFD) is the most suitable numerical tool. The high fidelity Direct numerical simulation (DNS), in principle capable of simulating all turbulent scales in the wake, comes with prohibitively high computational costs. As a relevant alternative, the conventional Reynolds-averaged Navier–Stokes (RANS) approach, which models all the turbulent scales, can be considered reliable for estimating blade loads and replicating certain global parameters of the near wake, but its degree of fidelity diminishes in the far wake where turbulent mixing and diffusion prevail. In this context, the Large-Eddy Simulation (LES) approach was developed as an intermediate approach between DNS and RANS. In LES, the large scales of turbulent flow are explicitly simulated, and the small scales dominated by viscous effects are modeled, providing detailed spatial and temporal information in the so-called 'inertial' range of turbulence [1]. In this context, a highly promising modeling approach emerges, offering an equilibrium between accuracy and computational efficiency. This approach involves integrating the Large Eddy Simulation (LES) technique for flow modeling with the Actuator Line Model (ALM) approach for simulating turbine rotors. In ALM, the turbine blades are substituted by distributed volume forces, thus reducing substantially the computational cost of the simulation by eliminating the need of resolving the detailed flow around (and near) the blades.

The ALM-LES has been utilized in prior research studies to analyse wake characteristics in scenarios involving a single, fixed-bottom turbine ([2], [3], [4],[5], [6]) or multiple fixed-bottom turbines in tandem layout ([7], [8]). Some studies have demonstrated the impact of turbulence models and inlet turbulence through the comparison of various codes ([9], [10], [11], [12], [13]). Finally, some studies have applied the ALM-LES approach to analyse complex cases involving combined platform motions and wake control or regulation techniques ([14], [15], [16], [17]). In this context, the primary aim of this paper is to analyse simple scenarios featuring both a fixed-bottom turbine and a surge platform motion. This analysis considers a laboratory model for which wind tunnel measurements in the near wake are available for reference. A comparison between RANS and LES calculations is performed in order to evaluate the different resolution capabilities of these two approaches and define the range of applicability for the RANS approach. This comparative analysis is also fundamental to emphasize the influence of platform motion on wake dynamics.

2. Test cases

The cases studied in this work were selected from the UNAFLOW experimental campaign, documented in [18] and [19]. A 1:75 scaled wind turbine model of the DTU 10 MW was tested within the Grande Galleria del Vento of the Politecnico di Milano (GVPM). The turbine, with a diameter of 2.38 m, features a twist distribution and a tapered chord variation, and null cone angle and null tilt. The blade was designed to align the model thrust coefficient with its full-scale counterpart, according to the approach introduced in [20]. Comprehensive 2D aerodynamic coefficients were evaluated in a 2D section of the DTU Red Wind Tunnel [18], spanning Reynolds numbers from 50k to 200k. The wind tunnel, measuring 13.84 m x 3.84 m with a length of 35 m, was operated to maintain a constant free-stream velocity of 4 m/s. Turbulence intensity at the inlet is below 2%, with an air density ρ =1.18 kg/m^3. Notably, a blockage effect manifested along the height, attributed to both rotor presence and wake confinement. For this reason, the present CFD simulations were performed in the actual wind-tunnel configuration.

Among all the cases tested in the experimental campaign, this article specifically analyses only two cases: the fixed-bottom case (called LC1.1) and the case with platform surge motion (called LC2.5). In both cases, the turbine rotates at a constant angular speed of 240 rpm with a free-stream velocity U_0 = 4 m/s, corresponding to a rated tip speed ratio of 7.5. The surge motion is imposed with a sinusoidal law that induces an initial windward translation of the turbine. The surge LC2.5 case is characterised by a platform frequency of 1 Hz and an amplitude of 0.035 m. The apparent wind experienced by the rotor (U_{app}), resulting from the vectorial combination of the free-stream velocity and the platform motion (x_s), serves as the reference velocity for assessing the rotor operational state. In the LC2.5 scenario, the surge motion causes a velocity excursion ranging from -0.22 m/s to 0.22 m/s, as depicted in Fig. 1 along with the corresponding platform displacement.

Journal of Physics: Conference Series **2767** (2024) 052050 doi:10.1088/1742-6596/2767/5/052050

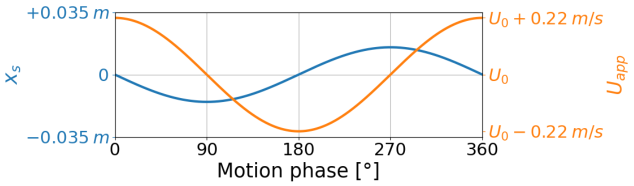

Figure 1. Surge platform motion (x_s) and apparent wind velocity (U_{app}).

3. Numerical method

3.1. Actuator Line Model

This study employs a version of the medium-fidelity ALM, originally proposed by Sørensen [21] and recently implemented by the authors in the OpenFOAM environment with a novel formulation, whose detailed description, validation and verification are documented in [22]. Within the ALM, the traditional blades are replaced by distributed volume forces along actuator lines, thus circumventing the need to resolve the blade boundary layer. The aerodynamic force computation employs look-up tables, whose interrogation requires the evaluation of the attack angle and Reynolds number. These parameters are based on the local relative velocity, which relies on the velocity sampled from the flow around the actuator point. In this formulation of the ALM, the velocity sampling is tackled through an innovative vortex-based approach [22]. This involves the analytical calculation of the induction resulting from the bound vorticity connected to the applied lift force. The induced velocity components, related to the lift force, are evaluated using the Biot-Savart law and subtracted from the sampled velocity to yield a final velocity without the induction effect of the bound vortex. A detailed explanation of the method can be found in [22].

Equation 1 represents the momentum equation solved within the OpenFOAM framework with the addition of the volumetric force, $\mathbf{f}$, that emulates the presence of the blades. The over-bar applied to the velocity $\mathbf{u}$ and the pressure p, signifies a time average in the RANS simulation and a spatial filtering in the LES simulation.

$$\frac{\partial \overline{\mathbf{u}}}{\partial t} + \overline{\mathbf{u}} \cdot \nabla \overline{\mathbf{u}} = -\nabla \overline{p} + \nu_{eff} \nabla \cdot (\nabla \overline{\mathbf{u}} + \nabla \overline{\mathbf{u}}^T) + \mathbf{f} \tag{1}$$

The effective turbulent viscosity, ν_{eff}, is composed of the molecular viscosity ν, and the turbulent viscosity ν_t. The turbulent viscosity is determined by the specific turbulence model employed, as better explained in section 3.3. For the LES model only the turbulence scales smaller than the cell size are modelled through a sub-grid turbulence model.

To prevent numerical issues, the volume force is spread throughout the domain using the convolution of a 2D Gaussian spreading function η_ϵ^{2D}, Eq. 2, as proposed by Mikkelsen [23].

$$\mathbf{f}_\epsilon = \mathbf{f} \otimes \eta_\epsilon^{2D}, \quad \eta_\epsilon^{2D}(d) = \frac{1}{\epsilon^2 \pi} \exp[-(d/\epsilon)^2] \tag{2}$$

where d is the distance from the force center point and ϵ is the semi-width of the force distribution that is set at twice the cell size, as recommended by Troldborg [24]. When extended to the physical three-dimensional domain, this regularization kernel adopts a cylindrical shape, providing an accurate representation of the blade finite length. Consequently, the current ALM tool can effectively resolve the vortices shed by the blade tip, by accounting for the drag caused by tip-vortex formation and mixing.

3.2. Computational domain and mesh

As previously mentioned, the aim of this study is to assess the wake resolution capability in both RANS and LES simulations. The LES modeling of the flow necessitates a finer mesh to capture smallest turbulence scales of the inertial range. Consequently, a less refined mesh was employed in RANS simulation and a more refined one in LES. The two numerical domains share the global dimensions to properly replicate the experimental configuration in the wind tunnel. The domain is extended downstream of the rotor up to 14.5D to ensure the complete development of the wake and to facilitate an in-depth analysis of the far wake. To address the blockage effect observed in the experimental campaign, the domain height was reduced by the boundary layer displacement thickness and a slip condition was applied on the wind-tunnel walls. No modifications were imposed on the side walls due to their negligible blocking effect, and a slip condition is enforced. At the inlet, a uniform free-stream velocity of 4 m/s was specified, while atmospheric pressure was assigned at the outlet. The mesh adopted in the RANS simulation was assessed after a grid dependence analysis, as documented in [22]. The mesh for RANS is structured as a Cartesian grid, comprising a total of 11.4 million hexahedral cells. The characteristic cell size of $\Delta = 0.0174$ m around the rotor is obtained by overlapping two cylindrical refinement zones, resulting in the layout illustrated in Fig. 2a, where only the zoomed area around the rotor is shown.

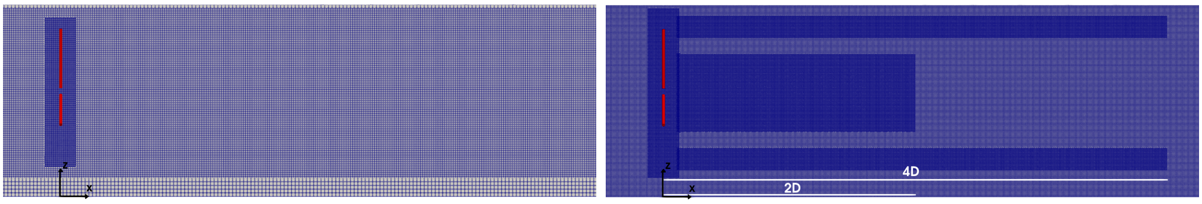

(a) RANS (b) LES

Figure 2. Zoom on the refinement around the rotor region for RANS and LES simulation.

Conversely, the LES simulation aims to attain a sufficiently refined mesh to enable the solver to resolve at least 80% of the total turbulent kinetic energy. A verification was performed on the mesh adopted to ensure the achievement of this goal. Therefore, it is necessary to reduce the global cell size and add two cylindrical refinement zones at the tip and hub of the blades, so to ensure an accurate representation of the corresponding vortices. The resulting mesh, composed by a total of 93.2 million cells, is reported in Fig. 2b and features a characteristic cell size in the areas of maximum refinement of 0.01 m, corresponding to $R/\Delta = 120$. This refinement level is consistent with that documented in similar papers reported in literature, such as Nilsson et al. [4], where a ratio of $R/\Delta = 122$ was applied, and Churchfield et al. [25] and Blaylock et al. [26] who use $R/\Delta > 100$. Finally, the blades are discretized with 75 actuator points.

3.3. Numerical solver

To capture the unsteady effects arising from both surge motion and blade rotation, the RANS simulation employs an unsteady solver, incorporating the $k - \omega SST$ turbulence model to characterize turbulent viscosity. In the LES simulation, turbulence is simulated up to the scales allowed by the maximum mesh refinement. For smaller scales, the subgrid-scale model is activated, establishing $\nu_t = \nu_{SGS}$. In this study, the subgrid-scale model follows the standard Smagorinsky formulation with a constant $C_s = 0.168$. This particular model is selected as a standard approach, well-suited for an initial evaluation of crucial turbulence aspects. Future investigations will explore different models to evaluate potential effects on wake resolution.

After establishing the turbulence models for the RANS and LES simulations, it is relevant to discuss the prescribed turbulence properties at the domain inlet. In the wind tunnel experiments, very low turbulence characterizes the incoming flow (below 2%); this value is sufficiently low to assume a laminar flow at the inflow boundary for the LES, leaving to the simulation model to reproduce the turbulent scales generated in the wind-tunnel chamber. In the RANS simulation, however, the assignment of a laminar inflow is not recommended for the peculiar feature of the two-equation turbulence model, so a turbulence intensity of 2% was set at the inlet.

The coupling of pressure and velocity is achieved using the PIMPLE algorithm available in OpenFOAM in both the RANS and LES simulations. This algorithm employs two inner loops to accelerate convergence and two outer loops to guarantee the convergence of the implicit velocity sampling technique. The time step was chosen so to satisfy the condition that the actuator line should not cross more than one cell per time step, resulting in a time step $\Delta t = 5.00 \times 10^{-4}$ s. In the RANS simulation, this limitation yields a Courant number below 0.5. In the LES case, the Courant number is slightly higher due the smaller cell size, but it remains always below 1, thus being adequate for accurately simulating the temporal scale of tip vortices with 4 time steps.

4. Experimental validation on turbine loads

Prior to delving into the examination of the wake, a validation of the ALM predictions is conducted. This validation involves a comparison of global loads with the correspondent experimental data acquired from the UNAFLOW campaign.

First considering fixed-bottom case, Table 1 reports the mean thrust and torque of the LC1.1-RANS simulation, LC1.1-LES simulation and experiment. RANS and LES simulations produce highly similar outcomes for both thrust and torque, as the RANS simulation adeptly captures the average flow characteristics. The mean thrust is accurately estimated, displaying deviations from the experiment by -0.5%. Regarding torque, the simulation slightly underestimates the mean value, with an error of -5%, corresponding to an absolute difference of $-0.17\,\mathrm{N\,m}$.

Table 2 provides both the mean value and peak-to-peak amplitude of thrust and torque for LC2.5 case. As in the previous scenario, RANS and LES simulations produce consistent results, featuring minimal discrepancies for both the mean value and amplitude of the thrust. Errors slightly increase to -6% and -4%, respectively, for the mean value and amplitude of the torque. However, these discrepancies in torque remain negligible when viewed in absolute terms, especially when factoring in the uncertainty associated with the load cell; in particular, torque experimental data may be affected by a slight rotor over-speed resulting from the non perfectly strict control logic of the controller, as identified during the UNAFLOW campaign [27].

Table 1. LC1.1: Experimental validation.

LC1.1	Thrust [N]	Torque [Nm]
Exp.	35.91	3.32
RANS	35.73	3.18
% error Exp.	-0.50	-4.16
LES	35.60	3.15
% error Exp.	-0.87	-5.12

Table 2. LC2.5: Experimental validation.

LC2.5	Thrust [N]		Torque [Nm]	
	Mean	Ampl.	Mean	Ampl.
Exp.	36.17	4.34	3.39	1.14
RANS	35.74	4.59	3.19	1.03
% error Exp.	-1.19	+0.67	-6.00	-3.15
LES	35.75	4.38	3.17	0.99
% error Exp.	-1.16	+0.11	-6.73	-4.24

The validation study indicates that the numerical simulations exhibit a good consistency with the experimental findings, thus indicating the proper ALM predictions of the rotor aerodynamics.

5. Wake analysis

After having assessed the code for the load prediction, the capability of the ALM to simulate the wake development and mixing is here reported, together with an experimental validation with the data available from the UNAFLOW test campaign [28].

The wake assessment is based on hot-wire velocity measurements performed in crosswind and stream-wise (along-wind) directions. The location of the hot-wire probes is summarised in the OC6 Phase III Definition document [29]. The experimental data were analysed by conducting a phase-locked averaging procedure using a time window equivalent to the characteristic period (revolution period for LC1.1 and surge period for LC2.5). For both scenarios, LC1.1 and LC2.5, the direct comparison between RANS and LES simulation is proposed to highlight the different accuracy in simulating the wake.

5.1. Crosswind

The crosswind measurements were conducted with hot-wire probes located at x/D = 2.3 downstream along the transversal direction of the wind tunnel flow at the hub height. In all the following figures the black dashed line represents the experiment, while the orange one the RANS simulation and the blue one the LES simulation.

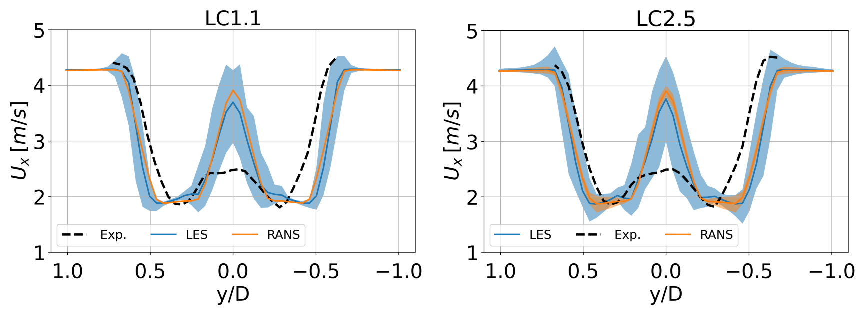

(a) (b)

Figure 3. Crosswind velocity profile at hub height and x/D=2.3.

Figure 3a displays the stream-wise velocity profile along the crosswind line for the LC1.1 case, viewed from upstream. The solid lines represent the mean velocity calculated over the last 3 seconds of the simulations, corresponding to 12 rotor revolutions. Meanwhile, the shaded areas illustrate the maximum and minimum velocity during these periods, capturing the unsteadiness in the wake. Firstly, simulations conducted with ALM do not model the turbine nacelle, thereby influencing the evolution of the near wake in the hub region. As depicted in the figure, both experiments and simulations capture a blockage effect, leading to a velocity higher than the upstream wind (4 m/s) at the lateral extremes. The absence of the nacelle in numerical simulations, causing an increase in velocity in the hub region, along with the need to match the mass flow observed in experiments, results in a decrease in axial velocity at the extremes compared to experimental outcomes. The absence of variability in the RANS simulation indicates that, at a distance of 2.3D from the rotor, any deterministic unsteadiness effect induced by the blade passage is no longer present. Consequently, the blue area, as captured by LES, represents the pure unsteadiness inherently associated to turbulence in the flow.

In Fig. 3b, the stream-wise velocity profile along the same crosswind line is analysed for the LC2.5 simulation. The solid lines represent the mean velocity calculated over the last 3 seconds, equivalent to 3 surge periods, with the correspondent velocity variability shown by the shaded areas. Concerning the influence of the nacelle and the blockage effect, similar considerations from the previous case can be repeated. The primary distinction in this scenario relates to the unsteadiness of the wake. Specifically, in the LC2.5 case, the RANS simulation exhibits variations in velocity around the rotor blades (from y/D = 0.04 to y/D = 0.5), corresponding to the deterministic perturbation effect of the surge motion, which remains evident at a distance of 2.3D. The shaded areas in the LES, therefore, encompass both the deterministic unsteadiness

 doi:10.1088/1742-6596/2767/5/052050

and the inherent unsteadiness of the turbulent flow. In conclusion, mean velocity profiles are properly captured by both the RANS and LES calculations.

To capture the fluctuations in wake velocities caused by the surge motion, only for LC2.5, Eq. 3 is employed to calculate the wake deficit (WD).

$$WD = \frac{\sum_{i=1}^{n} |r_i| (U_x - U_0)}{\sum_{i=1}^{n} |r_i|} \tag{3}$$

where r_i is the i-th radius along the cross-wind direction, U_x is the stream-wise velocity and U_0 the free-stream one. This parameter is computed along the crosswind line at a distance of 2.3D downstream from the rotor, within the range of $y = [-1.6, 1.6]$ m. It provides a measure of the velocity deficit by assigning greater weight to external velocities to mitigate the impact of the absence of the nacelle in ALM simulations. Figure 4 shows the WD trend, subtracted by the corresponding mean value ($\overline{WD}$), throughout a surge period. The mean value is subtracted to enhance the clarity of comparison. The WD values are computed with the phase-locked average of the stream-wise velocity over the last six periods of surge.

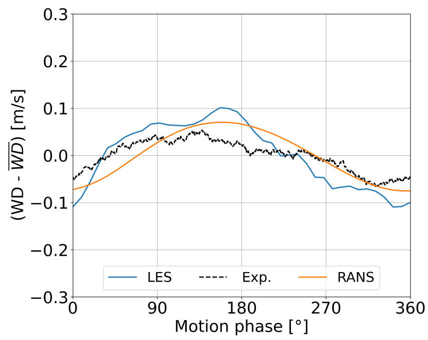

Figure 4. LC2.5: Wake deficit, shifted by the mean value, at x/D=2.3 over a surge period.

The ALM profiles exhibit a sound agreement with the measured data. Notably, the LES simulation appears to match more precisely the positions of both the maximum and the minimum of the experimental trend.

5.2. Along-wind

The assessment of the wake prediction in the streamwise direction is conducted by analysing experimental data obtained with hot wires placed along a line extending from x/D = 0.9 to x/D = 2.3 downstream of the rotor at a constant transversal position corresponding to y/R = 0.75 at the hub height. Simulations for all scenarios, LC1.1 and LC2.5, with both RANS and LES, are run up to 14 seconds to ensure a thorough development of the wake.

At first the fixed-bottom case LC1.1 is considered. Figure 5a shows the trends of axial velocity in the wake along the streamwise direction for the LC1.1 case. The continuous lines indicate the mean velocity over the last 12 revolution periods, with the shaded area illustrating the fluctuation in axial velocity between its maximum and minimum values. The LES and RANS simulations yield similar axial velocities in the near wake up to x/D = 3.65. A slight difference is noted when compared to experimental data, which appear to anticipate the velocity upturn point. Nevertheless, this difference remains relatively modest and likely falls within the uncertainty range of the experimental data.

Moving towards the far wake, more pronounced distinctions emerge between the two models. However, overall, the RANS simulation adeptly captures the mean velocity trend, providing

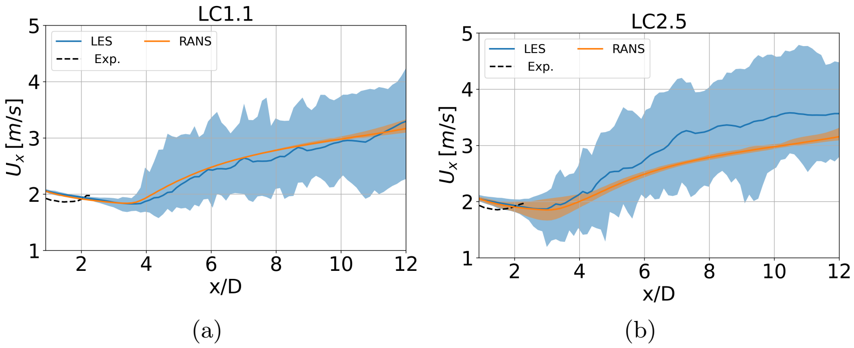

Figure 5. Mean value and amplitude of the axial velocity, y=0.75R.

a consistent estimation of the mean wake recovery. The LES simulation provides additional information on the flow unsteadiness: from x/D = 4 onward, the velocity fluctuation increases, indicating a rise in the turbulence intensity of the flow as the far wake develops. This study collocates the end point of the near wake in the point of reversal in the axial velocity trend, where the mixing phenomenon begins to predominate, as indicated by the increase in velocity variability. According to this approach, the near wake extension in LC1.1 case reaches x/D = 3.6 for RANS and x/D = 3.8 for LES.

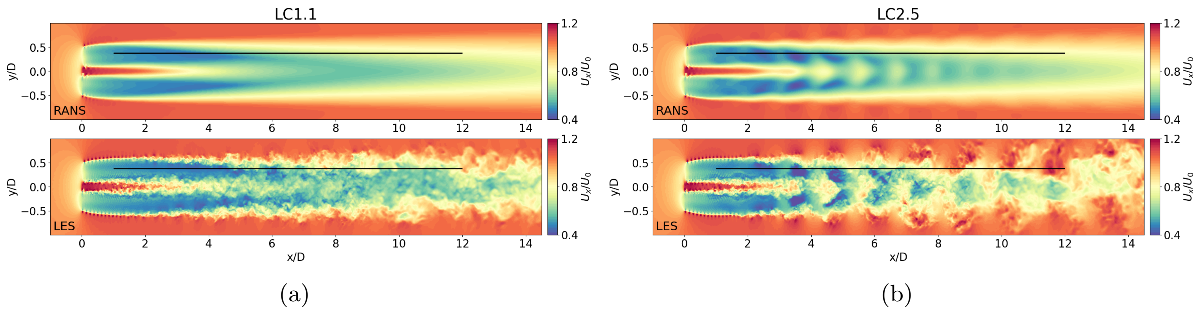

Figure 6. Instantaneous axial velocity field on a horizontal plane at hub height.

Figure 6a shows the flow field on the horizontal plane at hub height for the fixed-bottom RANS and LES simulations, together with the along-wind line guiding this analysis. As expected from the high fluctuations commented before, the LES simulation effectively captures the turbulent flow unsteadiness and reproduces in more detail the streamwise mixing of the tip vortices. Conversely, the RANS simulation accurately captures the average flow but falls short in reproducing the finer details of the wake, such as the tip vortices, due to the coarser mesh.

The same analysis is proposed for the surge motion case LC2.5 (Figure 5b). While the near wake shows comparable results between LES and RANS, more pronounced disparities become evident in the far wake. Notably, RANS predicts a more gradual velocity recovery beyond x/D=3 and foresees a velocity fluctuation attributed solely to platform motion (orange shaded area). The LES simulation reproduces an increased turbulence compared to the LC1.1 scenario, with significant subsequent changes in the mean velocity profile. Conversely, the RANS simulation LC2.5 falls short in simulating flow instability, resulting in an estimated mean velocity profile closely matching the one of the LC1.1 case. In LC2.5 case, the estimated near wake length is 3.27D for RANS and 3.04D for LES.

Figure 6b shows the axial velocity field on the horizontal plane at hub height for the LC2.5 case, including the along-wind line guiding the analysis. At the represented instant, the turbine is moving windward. The complex pattern of the wake produced by the surge motion becomes evident starting at x/D = 3. The RANS simulation effectively captures these features in the average velocity up to a distance of 6D before experiencing a severe mixing in the far wake.

The lack of experimental data in the far wake, makes the validation of the LES simulation not possible. However, in this work, the LES approach is considered intrinsically more reliable due to its high-fidelity reproduction of large scales of turbulence. Therefore, this analysis emphasizes the significance of employing LES simulations to explore the interaction among tandem turbines, especially in scenarios involving platform motion. Even within the fixed-bottom case, the introduction of a second turbine in the far wake reveals that the RANS simulation would strongly approximate the mean flow approaching the second turbine, not capturing the pronounced velocity fluctuations illustrated by the blue area in Fig. 5a, a phenomenon successfully captured by the LES simulation. In scenarios of surge motion, the RANS simulation not only falls short in capturing the intense flow variability but also yields an underestimation of the mean velocity profile. Therefore, the RANS simulation demonstrates adequacy in estimating the mean wake velocity in the fixed-bottom scenario, but lacks accuracy in assessing the instantaneous flow variability. Moreover, when examining the platform floating motions, the RANS simulation exhibits a greater deviation from the LES one in terms of mean value and shows a lack of capacity in effectively capturing the intricate flow structures.

5.3. Wake evolution

The wake evolution is now studied in terms of normalized stream-wise velocity and turbulence intensity across several transversal lines along the numerical domain, from 1D to 11D downstream of the rotor. The turbulence intensity is defined as the ratio between the standard deviation of the stream-wise velocity $std(U_x)$ and its mean value $\overline{U_x}$ (Eq. 4):

$$TI = \frac{std(U_x)}{\overline{U_x}} \tag{4}$$

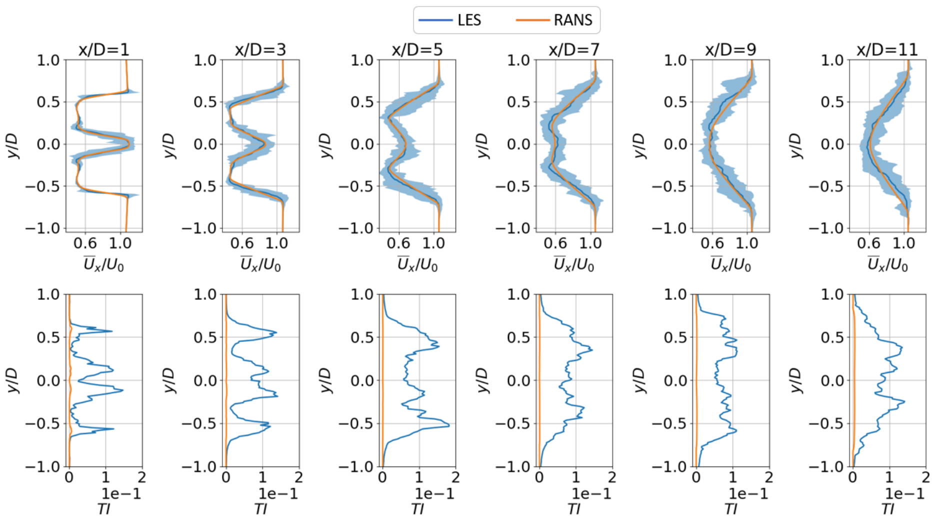

Figure 7. LC1.1: Normalized stream-wise wake velocity and turbulence intensity in xy plane.

Figure 7 is referred to the LC1.1 case. The mean velocity profiles (upper frames) of RANS and LES result consistent for all the sections, as already shown in Fig. 5a. The LES simulation captures a turbulence intensity that is not simulated in the RANS case. Close to the rotor, the peaks of TI appear in regions of high mean-flow gradients, in correspondence of the tip and hub vortexes, while the peaks move towards the wake core in the far wake as a result of the smearing of mean-flow gradients and turbulent mixing.

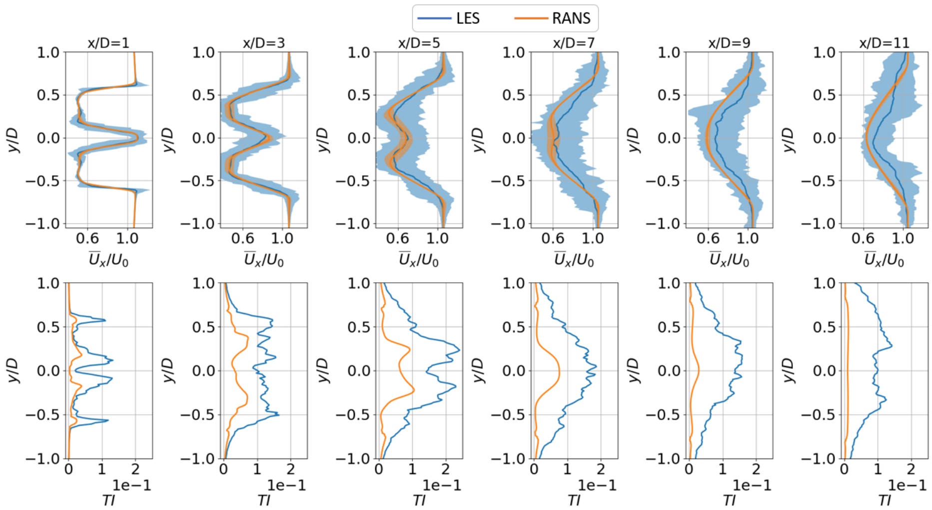

Figure 8. LC2.5: Normalized stream-wise wake velocity and turbulence intensity in xy plane.

Figure 8 illustrates a parallel analysis for the LC2.5 case. Noticeable discrepancies emerge between the streamwise velocity profiles of RANS and LES simulations. The RANS simulation indicates a more gradual mean recovery of the wake, as confirmed by Fig. 5b. Compared to the LC1.1 case, the RANS simulation yields higher values of turbulence intensity (TI), attributed to the influence of surge motion and discernible up to x/D = 7. Also in this scenario, TI peaks in the LES simulation, appear at hub and tip vortices and gradually move towards the core of the wake once the mixing effect becomes predominant.

5.4. Surge motion effects on wake recovery

After analyzing modeling aspects, this section focuses on the influence of surge motion on wake development, recovery, and turbulence, as predicted by high-fidelity simulations. Figure 9 depicts the trend of mean velocity along the previously examined along-wind line, accompanied by its variability (shaded areas).

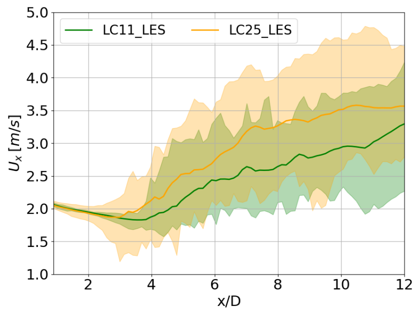

Figure 9. LES LC2.5 and LC1.1: Mean value and amplitude of the axial velocity, y=0.75R.

Notably, surge motion, while imparting a limited effect immediately downstream of the rotor, promotes a faster recovery of the mean velocity and increases its variability in the far wake, thereby reducing the extent of the near wake. These observations are corroborated in Figure

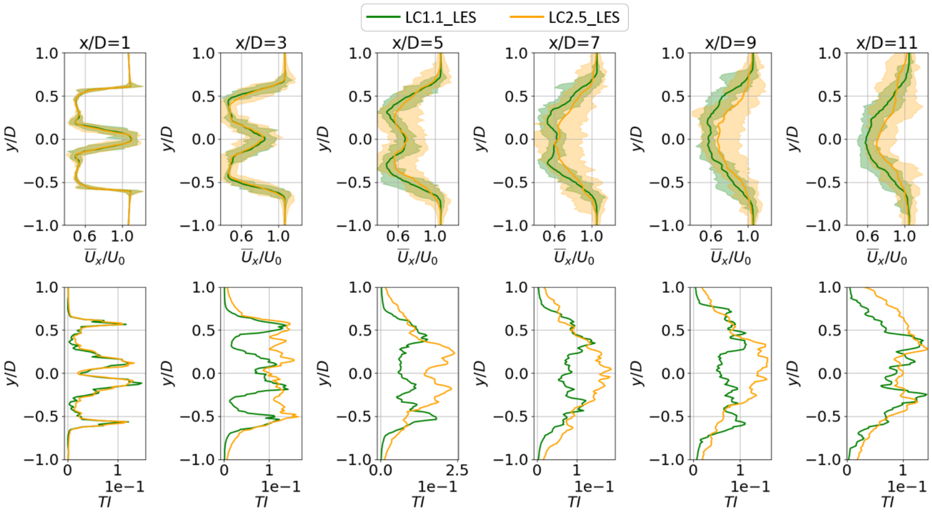

Figure 10. LES LC2.5 and LC1.1: Normalized stream-wise wake velocity and turbulence intensity in xy plane.

10, where mean velocity and TI profiles are reported along horizontal lines at various distances downstream of the rotor. LC2.5 simulation indicates an accelerated wake recovery from x/D = 5 onward, coupled with high TI values, unequivocally signifying a more pronounced diffusivity and thus a greater mixing phenomenon. Hence, the motion of surge gives rise to more extensive turbulent structures with prolonged persistence. These considerations suggest that a thorough exploration using LES model is necessary to accurately assess the instantaneous flow for a downstream turbine.

6. Conclusions

This paper has presented a study on the LES high-fidelity CFD simulation of the wake behind a turbine model for wind-tunnel experiments. Both fixed-bottom and surge-motion conditions have been analysed in comparison to both experiments and CFD simulations performed using the conventional Reynolds-average approach for turbulence modeling. The high-fidelity model, based on the large-eddy simulation approach, required a significant amount of computational resources, which however were limited to an affordable level thanks to the actuator-line modeling of the rotor aerodynamics, where the blades are replaced by volume forces. The RANS and LES calculation results were found to be in excellent agreement in terms of integral loads on the rotor, thus verifying the numerical approach, and in good agreement with the available experimental data, thus validating the selected models for the resolution of the rotor aerodynamics. Shifting focus to the analysis of the wake, the two models exhibit a good correspondence among each other and with the experimental data in the near wake region, predicting similar mean velocity levels and limited flow unsteadiness, even in the surge case. Significant differences, instead, emerge in the far wake region, where the high-fidelity simulations predict a steep rise in flow unsteadiness, both in the fixed-bottom and surge cases. This effect has a relatively minor impact on the mean velocity profile in the wake, and hence on the wake recovery, for the fixed-bottom case; conversely, in the surge case the higher turbulent unsteadiness alters the mean wake recovery. Eventually, the influence of the surge motion on the wake development and recovery was performed by comparing the LES results for the fixed-bottom and surge case. The surge motion showed a limited impact on the near wake, but promotes a rapid increase of velocity from x/D=3. In the far wake, the surge case presents greater mixing and faster recovery, as well as higher turbulence intensity. This great unsteadiness, which is expected to severely influence the aerodynamics and performance of a turbine placed downstream in wind-farm configuration, is completely absent in the RANS simulation, proving, also on the quantitative ground, the relevance of a high-fidelity modeling of the wake for wind-farm design and optimization.

Future works will involve exploring different sub-grid turbulent scale models to evaluate potential effects on wake resolution and implementing a more realistic turbulence condition on the inflow. Furthermore, an experimental campaign is planned to obtain additional wake measurements and achieve a more comprehensive validation of the simulations.

7. Acknowledgments

This study was carried out within the NEST - Network 4 Energy Sustainable Transition (D.D. 1243 02/08/2022, PE00000021) and received funding under the National Recovery and Resilience Plan (NRRP), Mission 4 Component 2 Investment 1.3, funded from the European Union - NextGenerationEU. This manuscript reflects only the authors' views and opinions, neither the European Union nor the European Commission can be considered responsible for them.

References

[1] Pope S B 2000 *Turbulent Flows* (Cambridge University Press)
[2] Martínez-Tossas L A, Churchfield M J and Leonardi S 2015 *Wind Energy* **18** 1047–1060
[3] Sørensen J N, Mikkelsen R F, Henningson D S, Ivanell S, Sarmast S and Andersen S J 2015 *Philosophical Transactions of the Royal Society A: Mathematical, Physical and Engineering Sciences* **373** 20140071
[4] Nilsson K, Shen W Z, Sørensen J N, Breton S P and Ivanell S 2015 *Wind Energy* **18** 499–514
[5] Parinam A, Benard P, von Terzi D and Viré A 2023 *Journal of Physics: Conference Series* **2505** 012039
[6] Gao Z, Li Y, Wang T, Ke S and Li D 2021 *Applied Mathematics and Mechanics* **42** 511–526
[7] Porté-Agel F, Wu Y T, Lu H and Conzemius R J 2011 *Journal of Wind Engineering and Industrial Aerodynamics* **99** 154–168
[8] Onel H C and Tuncer I H 2021 *Computers & Fluids* **220** 104872
[9] Martínez-Tossas L A, Churchfield M J, Yilmaz A E, Sarlak H, Johnson P L, Sørensen J N, Meyers J and Meneveau C 2018 *Journal of Renewable and Sustainable Energy* **10** 033301 ISSN 1941-7012
[10] Martínez-Tossas L A, Churchfield M J and Meneveau C 2015 *Journal of Physics: Conference Series* **625** 012024
[11] Sarlak H, Meneveau C and Sørensen J N 2015 *Renewable Energy* **77** 386–399
[12] Sarlak H, Meneveau C, Sørensen J N and Mikkelsen R 2015 *Direct and Large-Eddy Simulation IX* ed Fröhlich J, Kuerten H, Geurts B J and Armenio V (Cham: Springer International Publishing) pp 169–175
[13] Sarlak H, Pierella F, Mikkelsen R and Sørensen J N 2014 *Journal of Physics: Conference Series* **524** 012145
[14] Wang J, Wang C, Campagnolo F and Bottasso C L 2019 *Wind Energy Science* **4** 71–88
[15] Johlas H M, Martínez-Tossas L A, Schmidt D P, Lackner M A and Churchfield M J 2019 *Journal of Physics: Conference Series* **1256** 012018 URL `https://dx.doi.org/10.1088/1742-6596/1256/1/012018`
[16] Wang J, Wang C, Castañeda O D, Campagnolo F and Bottasso C L 2018 *Journal of Physics: Conference Series* **1037** 072032 URL `https://dx.doi.org/10.1088/1742-6596/1037/7/072032`
[17] Yang L, Liao K, Ma Q, Ma G and Sun H 2023 *Renewable Energy* **218** 119255
[18] Fontanella A, Bayati I, Mikkelsen R, Belloli M and Zasso A 2021 *Wind Energy Science* **6** 1169–1190
[19] Bayati I, Belloli M, Bernini L, Boldrin D, Boorsma K, Caboni M, Cormier M, Mikkelsen R, Lutz T and Zasso A 2018 *Journal of Physics: Conference Series* **1037** 072037
[20] Bayati I, Belloli M, Bernini L, Giberti H and Zasso A 2017 *IET Renewable Power Generation* **11** 1120–1126
[21] Sorensen J N and Shen W Z 2002 *J. Fluids Eng.* **124** 393–399
[22] Persico G, Sanvito A, Firpo A, Schito P, Dossena V and Zasso A *Available at SSRN 4625595*
[23] Mikkelsen R *et al.* 2003 *Actuator disc methods applied to wind turbines* Ph.D. thesis PhD thesis, Technical University of Denmark
[24] Troldborg N 2009 *Actuator Line Modeling of Wind Turbine Wakes* Ph.D. thesis
[25] Churchfield M J, Schreck S, Martinez-Tossas L A, Meneveau C and Spalart P R
[26] Blaylock M L, Martinez-Tossas L, Sakievich P, Houchens B C, Cheung L, Brown K, Hsieh A, Maniaci D C and Churchfield M J URL `https://arc.aiaa.org/doi/abs/10.2514/6.2022-1921`
[27] Bergua R, Robertson A, Jonkman J, Branlard E, Fontanella A, Belloli M, Schito P, Zasso A, Persico G, Sanvito A *et al.* 2022 *Wind Energy Science Discussions* **2022** 1–33
[28] Robertson A URL `https://www.osti.gov/biblio/1922900`
[29] Robertson A, Bergua R, Fontanella A and Jonkman J URL `https://www.osti.gov/biblio/1957538`